Phonon dispersion and lattice dynamics of $KTaO_3$ from 4 to 1220 K

C. H. Perry
Department of Physics, Northeastern University, Boston, Massachusetts 02115
and Hochfeld-Magnetlabor, Max-Planck-Institut, 38042 Grenoble CEDEX, France

R. Currat
Institut Max Laue–Paul Langevin, Boîte Postale 156X, 38042 Grenoble CEDEX, France
and Brookhaven National Laboratory, Upton, New York 11973

H. Buhay*
Department of Physics, Northeastern University, Boston, Massachusetts 02115

R. M. Migoni†
Departamento de Materiales, Comisión National de Energia Atómica, Buenos Aires, 1492 Buenos Aires, Argentina

W. G. Stirling‡
Institut Max Laue–Paul Langevin, Boîte Postale 156X, 38042 Grenoble CEDEX, France

J. D. Axe
Brookhaven National Laboratory, Upton, New York 11973
(Received 7 April 1988; revised manuscript received 21 November 1988)

A complete set of transverse and longitudinal phonon branches in each of the three principal directions (⟨100⟩, ⟨110⟩, and ⟨111⟩) and polarizations have been measured up to 60 meV in the cubic perovskite $KTaO_3$. Results were obtained at 296 K and at several other temperatures between 4 and 1220 K. The data have been analyzed in terms of a shell model which includes a fourth-order core-shell interaction at the O^{2-} ion. Within the self-consistent mean-field approximation a very accurate description of the lattice dynamics over the whole temperature range is obtained. It is shown that the nonlinear polarizability of O^{2-} along the Ta—O—Ta chains is primarily responsible for most of the phonon shifts, particularly of the ferroelectric soft mode, and for the strong second-order Raman effect.

I. INTRODUCTION

$KTaO_3$ undergoes no ferroelectric phase transition like $BaTiO_3$ (Ref. 1) and $KNbO_3$ (Ref. 2) but its dielectric constant increases rapidly with decreasing temperature.[3] This cubic perovskite has been the object of many ir,[4–7] Raman,[8–11] inelastic-neutron-scattering,[12–14] and hyper-Raman[15] studies as its lowest long-wavelength optical phonon softens with decreasing temperature. It is prevented from becoming unstable near 0 K by the effect of quantum fluctuations; the instability of this so-called ferroelectric mode leads to the appearance of ferroelectricity in many oxide perovskites. Thus $KTaO_3$ is alternatively called a quantum paraelectric[16] or an incipient ferroelectric. It is a model system to study soft-mode behavior[17] and phonon-phonon mode interactions[18] with temperature as it retains its cubic space-group symmetry O_h^1 ($Pm3m$) at all temperatures.

The ferroelectric soft mode in $KTaO_3$, as well as in $SrTiO_3$, has been shown to originate from the nonlinear anisotropic behavior of the O^{2-} polarizability.[19] This mechanism was found also to be responsible for the intense second-order Raman scattering in these crystals. All this was demonstrated in the context of a self-consistent shell-model description of the lattice dynamics.[20] The theory predicted the temperature dependence of the phonon branches, and it correctly accounted for the anomalous softening of the TA branch in the ⟨100⟩ directions[13] and the TO-TA phonon coupling.[14] However, the model parameters were limited by the lack of experimental data available at that time as only the zone-center modes and a few low-energy phonon branches had been measured. The extensive neutron studies reported here allow a more exact determination of the shell-model parameters for $KTaO_3$ to be made. In addition the temperature-dependent studies provide a more stringent test of the model over a wider temperature range. To a large extent the model correctly accounts for the observed temperature dependence of most of the phonon branches.

Previous inelastic-neutron measurements[12–14] were only concerned with the transverse-acoustic and lowest-energy transverse-optic dispersion curves along the ⟨100⟩ and ⟨110⟩ directions. Comès and Shirane[14] reported significant energy shifts for phonons propagating along ⟨100⟩ as the temperature was decreased. At low temperatures, an acoustic-optic mode interaction was

shown to be the main cause of the observed strong anisotropy of the low-lying branches. The dielectric response derived from far-infrared (FIR) reflectance studies[4–7] at temperatures between 10 and 500 K showed that the soft "ferroelectric" mode in $KTaO_3$ is underdamped and is anharmonically coupled to other Γ-point transverse-optic modes.[4–6,18] Electric-field-induced Raman[10] and hyper-Raman[15] measurements on the other hand yield much smaller values of the damping constants, especially for the soft mode. The effect of surface layers[21,22] strongly influence the FIR reflectivity data due to the small penetration depth, whereas light-scattering and neutron-scattering techniques each probe bulk properties and potentially provide more realistic values.

In this paper we present the most complete set of experimental measurements of the phonon dispersion curves of $KTaO_3$ observed at room temperature; they supplement and greatly extend those undertaken previously. The data were taken on triple-axis neutron spectrometers at the Institut Max Laue–Paul Langevin, Grenoble, and Brookhaven National Laboratory, Upton, NY. The results are compared with those reported for $SrTiO_3$ (Refs. 23–25) and with the original dispersion curves calculated by Migoni *et al.*[19]

The low-energy dispersion curves that showed the largest shifts at low temperature have been remeasured; the improved resolution used in our work provided more reliable spectral line shapes. All phonon branches propagating in the three principal directions ⟨100⟩, ⟨110⟩, and ⟨111⟩ have been investigated up to 60 meV at several temperatures between 4 and 1220 K. The zone-center and zone-boundary modes were examined in particular detail. In cases where there is a significant overlap of the scattering profiles of modes of the same symmetry, the neutron data display anomalous phonon line shapes due to anharmonic mode coupling,[26–30] similar to those observed in $q \simeq 0$ FIR and Raman studies.[4–10]

In the theoretical section we summarize the main features of the self-consistent shell model.[19] This is followed by a calculation of the dispersion curves at room temperature, for which we have detailed data on all but the highest branches. The previously determined parameters[19,20] were readjusted in order to eliminate some discrepancies and make use of additional phonon information not available in the earlier calculations. After this, we perform a self-consistent calculation of the phonon frequencies at all temperatures measured, whereby a value of the fourth-order core-shell coupling parameter at the O^{2-} ion is obtained. This is the only nonlinear parameter of the theory. Then we recalculate the second-order Raman spectra arising from the corresponding nonlinear O^{2-} polarizability and compare them with experimental spectra. Finally, we calculate the phonon frequency distribution and the lattice specific heat.

II. EXPERIMENTAL DETAILS

The high quality $KTaO_3$ single crystal was grown by A. Linz, MIT; its dielectric properties and far-infrared dispersion have been measured previously and reported elsewhere.[7] It was a large square plate ($2.5\times2.3\times0.3$ cm^3) which had the ⟨100⟩ axes aligned along the face edges.

Extensive inelastic-neutron-scattering measurements were taken at the high-flux reactor at the Institut-Laue-Langevin (ILL-HFR), Grenoble, France, and at the High Flux Beam Reactor at Brookhaven National Laboratory (BNL-HFBR). The experiments were performed with the IN8 three-axis spectrometer at the ILL-HFR and with the H8 and H4M spectrometers at the BNL-HFBR. The experimental configurations used for the phonon measurements are summarized in Table I with collimations optimized to obtain the resolution necessary for each type of measurement. The scattered (E_1) or incident (E_0) neutron energies (see Table I) were chosen to minimize "spurious" processes involving higher order neutrons ($\lambda/2$, $\lambda/3$, etc.). Estimates of errors in the experimental values of the mode frequencies were calculated using $\Delta\nu=[(\Delta\nu_{\text{align}})^2+(\Delta\nu_\sigma)^2]^{1/2}$ where $\Delta\nu_{\text{align}}(\simeq 0.3\%E_0)$ is the error in the instrumental alignment and $\Delta\nu_\sigma$ is the variance of the least-squares fit of the mode frequency. Effects of the finite instrumental resolution were estimated using the method of Cooper and Nathans.[31]

In various experiments the sample was placed in a vacuum furnace or cryostat and oriented with either a [110]

TABLE I. Summary of the experimental configurations. The same $KTaO_3$ sample was used in the phonon dispersion measurements on the three different three-axis spectrometers.

	Instruments		
	IN8 (ILL-HFR)	H8 (BNL-HFBR)	H4M (BNL-HFBR)
Monochromator crystal(s)[a]	Cu(220)	PG(002),Be(110)	PG(002)
Analyzer crystal(s)	PG(002)	PG(002),PG(004)	PG(004)
Fixed energy (meV)			
Incident, E_0 (meV)		E_0: 14.5–50, 62–94	E_0: 13.5
Scattered, E_1 (meV)	E_1: 22.7–47.9		
Energy loss or gain	loss	loss	gain
Brillouin zones	(*hkh*)	(*hkh*),(*hk*0)	(*hkh*)
Temperatures (K)	296, 1220	4–1220	296, 1220

[a]PG refers to pyrolytic graphite.

or [100] crystal axis vertical. Phonon data were taken at 4.6, 20, 296, 435, 562, 810, 930, and 1220 K.

III. THE MODEL

The original model used by Cowley[23] and Stirling[24] for $SrTiO_3$ has been modified slightly to incorporate the anisotropic oxygen polarizability. It includes axially symmetric short-range forces which couple the shell of each oxygen ion to those of its nearest A, B, and O ions, where B (Ta in $KTaO_3$) denotes the ion at the center of the oxygen octahedra in the cubic perovskite ABO_3 structure. Both the A and B ions are considered isotropically polarizable, each one with a shell charge Y and a core-shell coupling constant K. However, since the oxygen polarizability depends strongly on its crystal environment, two independent core-shell force constants are considered for this ion: K_{OB} for core-shell displacements directed towards its neighboring B ions and K_{OA} for those lying in the plane where the oxygen is surrounded by four A neighbors; in what follows, the B and A components of any tensorial property of the oxygen ion will refer to the aforementioned direction and plane, respectively.

The lowest-order anharmonic core-shell interaction at the oxygen ion is of fourth order. It includes four independent parameters, $K_{OB,B}$, $K_{OB,A}$, $K_{OA,A}$, and $K_{OA,A'}$, where each A and B corresponds to a pair of core-shell displacements. This is a simple consequence of the oxygen site symmetry. However, the results obtained by considering only the interaction $K_{OB,B}$ are in very satisfactory agreement with the Raman spectra[8,9,19] and the temperature behavior of the lower-energy phonon branches[12–14,20] below room temperature, and they are not improved by including the nonlinear contributions related to any of the other three parameters. $K_{OB,B}$ is responsible for the modulation of the B component of the oxygen polarizability due to the core-shell polarization in the direction pointing towards B. This polarizability is strongly activated by the ferroelectric soft mode.

Within a mean-field approximation, Migoni *et al.*[19] have shown that an effective, temperature-dependent core-shell B spring constant is obtained, of the form

$$K_{OB}(T)=K_{OB}+\tfrac{1}{2}K_{OB,B}\langle W_{OB}^2\rangle_T\ , \tag{1}$$

where $\langle W_{OB}^2\rangle_T$ is the thermal average of the oxygen shell displacements in the direction pointing towards B. In terms of the shell eigenvectors $f_\alpha(O_\alpha;q,j)$ of the oxygen ion O_α whose neighboring B ions lie in the α direction, these shell displacements become

$$\langle W_{OB}^2\rangle_T = \frac{\hbar}{2NM_0}\sum_{q,j}[f_\alpha^2(O_\alpha;q,j)/\omega(q,j)]\coth\left[\frac{\hbar\omega(q,j)}{2kT}\right] \tag{2}$$

and the temperature-dependent ferroelectric mode (TO_1,Γ) frequency given by

$$[\omega_F^{\rm expt}(T)]\rightarrow[K_{OB}^{\rm expt}(T)]\rightarrow[\langle W_{OB}^2\rangle_T]\rightarrow[K_{OB}(T)]\ ,$$
$$\text{LSQF}\ \rightarrow\ K_{OB},K_{OB,B} \tag{3}$$

where f_0 is the shell eigenvector of that oxygen ion whose B ion neighbors lie in the direction of polarization of the ferroelectric mode and ω_0 is the (imaginary) harmonic mode frequency. $\omega_F(T)$ and $K_{OB}(T)$ are calculated self-consistently as described in Ref. 19.

IV. DISCUSSION AND RESULTS

A. Dispersion curves at room temperature

In Fig. 1 we summarize the room-temperature (296 K) phonon dispersion curves of $KTaO_3$ measured in the high-symmetry directions [100], [110], and [111]. The present data (solid circles) extend the results from prior work (open circles).[12–14] The previously determined phonon branches were remeasured and in all cases good agreement was obtained.

The group theoretical results for a cubic perovskite structure have been given by Cowley;[23] his notation will be used throughout this paper. The mode basis vectors were used to determine optimum positions in reciprocal space for the observation of each branch. For example, for phonons propagating in the Δ direction ($\mathbf{q}\|[010]$) group theory leads to five doubly degenerate transverse branches of Δ_5 symmetry, four longitudinal branches of Δ_1 symmetry, and one branch of Δ_2 symmetry. The Δ_5 phonons were measured in the (202), (313), and (303) Brillouin zones; the Δ_1 (LO_1 and LO_2) phonons in the (020) and (030) zones and the Δ_1 (LO_3) in the (044) zone. The Δ_2 mode was measured around the (160) zone. In the Σ direction ($\mathbf{q}\|[101]$) group theory gives 4 Σ_4, 5 Σ_1, 5 Σ_3 branches and a single Σ_2 branch. The Σ_4 and Σ_2 modes are transverse and the Σ_1 and Σ_3 modes are not purely transverse or longitudinal. In the Λ direction ($\mathbf{q}\|[111]$) there are 4 Λ_1, 1 Λ_2, and 5 Λ_3 modes which are not pure transverse or longitudinal. The branches with Λ_2 and Σ_2 representations and some of the high-energy branches (>60 meV) were not measured due to time limitations.

Anticrossing between branches of the same symmetry can be seen in the directions Σ and Λ in Fig. 1 and correspond to an exchange of eigenvectors between the two branches. In addition, anharmonic mode-mode coupling may lead to line-shape distortions as discussed in Sec. IV B below.

The calculated phonon branches are obtained by first fitting the measured phonon frequencies at room temperature using the initial parameter set for the model found previously.[19] A room-temperature (T_a) value of $K_{OB}(T)$, called $K_{OB}^{\rm expt}(T_a)$, is determined together with the fourteen other temperature-independent parameters (including two ionic charges, Z_A,Z_B).

The best fit dispersion curves are shown as solid lines in Fig. 1 and correspond to the final parameter values in

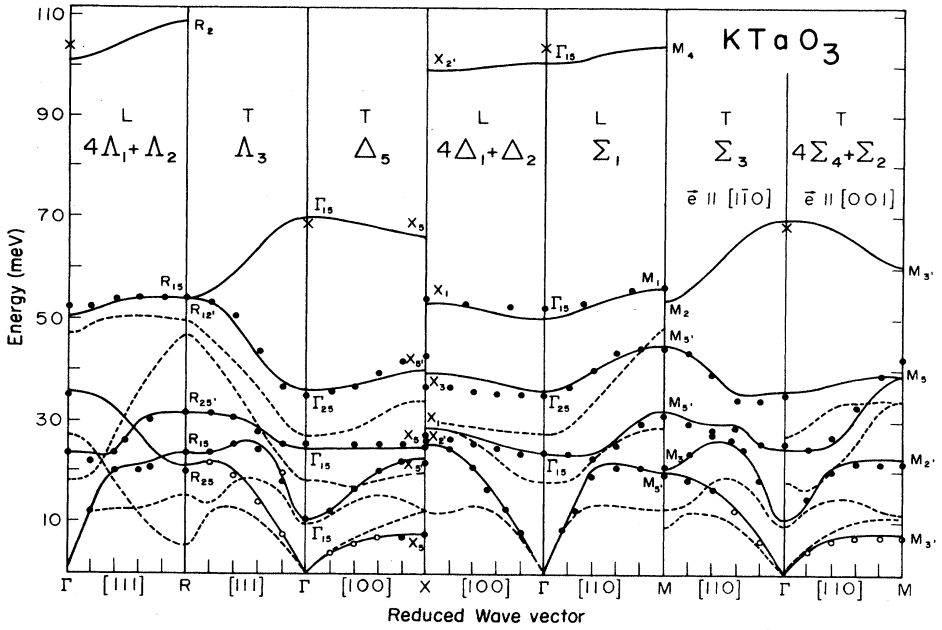

FIG. 1. Dispersion curves of $KTaO_3$ at room temperature. Experimental data: this work and Ref. 12 (●), Ref. 14 (○), and Refs. 4–10 and 15 (×). Solid lines: present calculations. Dashed lines: measured dispersion curves for $SrTiO_3$ (Refs. 24 and 25).

Table II. Here the longitudinal components of the interatomic force constants are denoted, as usual, by A and the transverse ones by B. The rest of the notation has already been explained. The highest TO and LO modes at the Γ point, whose experimental values are known from FIR-reflectivity measurements[4–6] and differential Raman spectroscopy,[11] were also fitted. A very satisfactory agreement between the calculated curves and the experimental data can be seen in Fig. 1. The irreducible representations of the phonons[19,23] are shown in Fig. 1 as given by the model and they agree with experimental observations.

The calculated ionic displacement amplitudes are given in Table III for all zone-center and zone-boundary modes which are not uniquely determined by symmetry. Experimental amplitude values are available for the $TO_1(\Gamma)$ mode[32] (shown in parentheses) only, and they agree very well with the calculated ones.

In Fig. 1 the calculated phonon frequencies of $KTaO_3$ (solid lines) can also be compared with those of $SrTiO_3$ (dashed lines).[19,23–25] It turns out that whenever the ionic motion for a given mode is dominantly an A (Sr^{2+} or K^+) or B (Ti^{4+} or Ta^{5+}) oscillation in both crystals, the frequency ratio is very closely given by the ionic mass ratio. Therefore, very similar effective forces are to be expected on the A and B ions in both crystals. In fact, from the comparison of the parameters for $KTaO_3$ with those for $SrTiO_3$, also shown in Table II, it can be seen that the short-range force constants between ion pairs O-A and O-B scale with the corresponding Coulomb interactions due to the replacement of Sr^{2+} and Ti^{4+} by K^+ and Ta^{5+}, respectively (the lattice constants of the two crystals differ by only 2%).

The model was not constrained to fit the elastic[14,33] and dielectric constants.[7,18] The expressions for the elastic constants in terms of the parameters are given in Ref. 23 and the high-frequency dielectric constant is numerically computed through the general formula [Eq. (2.44) in Ref. 34]. The calculated values for these quantities are compared with the experimental ones in Table IV; reasonable agreement is obtained.

B. Temperature-dependent studies

Detailed measurements of several branches were made as a function of temperature. The temperature depen-

TABLE II. Model parameters for $KTaO_3$ derived from a least-squares fit to the data shown in Fig. 1. The values can be compared with those for $SrTiO_3$ (Ref. 19).

	Force Constants $e^2/2v$						Charges e					Core-shell couplings e^2/v			
	A_{OA}	B_{OA}	A_{OB}	B_{OB}	A_{OO}	B_{OO}	Z_A	Z_B	Y_A	Y_B	Y_O	K_A	K_B	K_{OA}	$K_{OB}^{expt}(T_a)$
$KTaO_3$	14.65	−1.01	359	−68	3.22	1.085	0.82	4.84	−.419	7.83	−3.01	1000.0	1283.0	410.0	357.4
$SrTiO_3$	26	−4.25	285	−43	1.9	0.74	1.62	3.3	2.3	−1.5	−2.7	57	1446.0	624.0	98.97

TABLE III. Displacement amplitudes $u_\alpha(k)=e_\alpha(k)(m_k)^{1/2}$ for all zone-center and zone-boundary modes which are not uniquely determined by symmetry. The values in parentheses for the mode TO_1 (Γ_{15}) are experimentally determined (Ref. 32). Each oxygen is labeled with the direction of its nearest Ta ion. The amplitudes are normalized in such a way that the largest component equals 1. The ionic displacement for the Λ_3 modes given in Ref. 23 are incompatible with those at R, and there are errors in this respect in the paper by Stirling (Ref. 24) as well. The following relations between eigenvector components define two mutually orthogonal sets of eigenvectors corresponding to the doubly degenerate modes Λ_3, compatible with the modes Γ_{15}, Γ_{25}, R_{15}, R_{25}, R'_{25}, and R_{12}: $A_x=\pm A_y$; $A_z=-(A_x+A_y)$; $B_x=\pm B_y$; $B_z=-(B_x+B_y)$; $X_x=\pm Y_y$; $Z_z=-(X_x+Y_y)$; $Y_y=\pm Y_x$; $Y_x=-(X_z+Z_y)$; $Y_z=\pm X_z$; $Z_x=\pm Z_y$. The capital letter X, Y, or Z identifies an oxygen site whose fourfold symmetry axis lies in the x, y, or z direction, respectively. (Irr. rep. denotes irreducible representation.)

			K			T_a			O_z			O_y			O_x		
Point	Irr. rep.	Mode	X	Y	Z	X	Y	Z	X	Y	Z	X	Y	Z	X	Y	Z
Γ (0,0,ϵ)	Γ_{15}	TO_1	0.13 (0.12)			−0.28 (−0.27)			1 (0.91)			1 (0.91)			0.86 (1)		
$\epsilon\to 0$	($x\rightleftarrows y$)	TO_2	−1			0.14			0.26			0.26			0.28		
		TO_4	−0.01			0.01			0.45			0.45			−1		
		LO_1			1			−0.21			−0.08			0.02			0.02
		LO_3			0.15			0.13			0.18			−1			−1
		LO_4			−0.05			−0.08			1			0.02			0.02
X (00$\frac{1}{2}$)	X_5	TA				−1						0.22			0.03		
	($x\rightleftarrows y$)	TO_2				0.02						1			0.51		
		TO_4				0.01						0.50			−1		
	X'_5	TO_1	1						0.12								
	($x\rightleftarrows y$)	TO_3	−0.05						1								
	X'_2	LA			1						0.12						
		LO_4			−0.05						1						
	X_1	LO_1						0.95							1		1
		LO_3						−0.19							1		1
M ($\frac{1}{2}\frac{1}{2}$0)	M'_3	TA						1			0.02						
		TO_4						−0.002			1						
	M'_5	LA=TA		−1		0.26			0.21								
	($x\rightleftarrows y$)	$LO_1=TO_2$		0.75		0.56			1								
		$LO_2=TO_3$		0.07		0.13			−1								
R ($\frac{1}{2}\frac{1}{2}\frac{1}{2}$)	R_{15}	$LA=TO_1$	1							0.02			0.02				
		$LO_3=TO_4$	−0.01							1			1				

TABLE IV. Elastic and dielectric constants of $KTaO_3$.

	C_{11}	C_{44} (10^{12} dyn/cm^2)	C_{12}	ϵ_∞
Experiment	3.936[a]	1.071[a]	1.30[b]	4.3[c]
Calculated	4.35	1.19	1.04	4.6

[a]Reference 33.
[b]Reference 14.
[c]References 7 and 18.

dence of the low-frequency transverse branches is presented in Fig. 2. Appreciable positive shifts of the transverse phonon energies are observed as the temperature is raised. Even at the highest temperatures, all modes remained observable and underdamped. For example at room temperature the lowest transverse-optic (TO_1) mode for $q=(0.1,0,0.1)a^*$ has a frequency of 14 meV and a width of 2.1 meV. At 1220 K ($kT=105$ meV) it has a frequency of 17 meV and a width of 4 meV. In Fig. 2 it can be seen that the frequencies of the Δ_5 TA branch and the Σ_4 TA branch are exceptionally low at

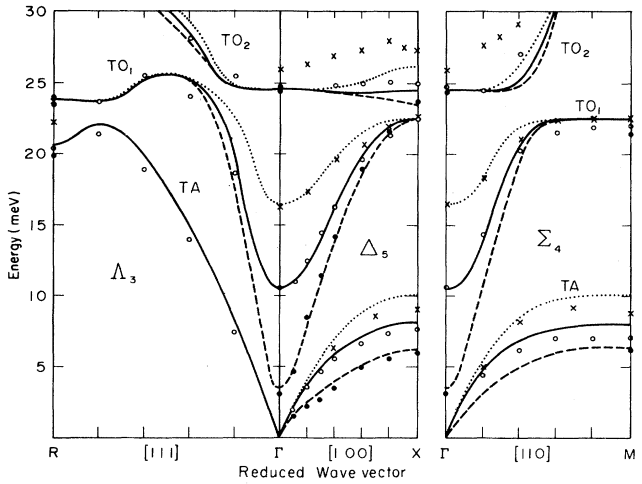

FIG. 2. Phonon branches which exhibit the most significant temperature shifts. The lines correspond to calculations and the points to measurements (present work and Refs. 12–14) at 20 K (– – –,●), 296 K (——,○), and 1220 K (· · · ·,×).

the zone boundary; earlier work on $KTaO_3$ and other perovskites have attributed this behavior to anharmonic mode coupling.[13,14]

In neutron-scattering studies of $BaTiO_3$ (Ref. 29) and $KNbO_3$ (Refs. 26 and 27) large anharmonic coupling between the TO_1 and TA modes has been observed. In these materials the soft mode is heavily damped and the scattering profiles display pronounced asymmetries due to anharmonic interference effects. In $KTaO_3$ we find

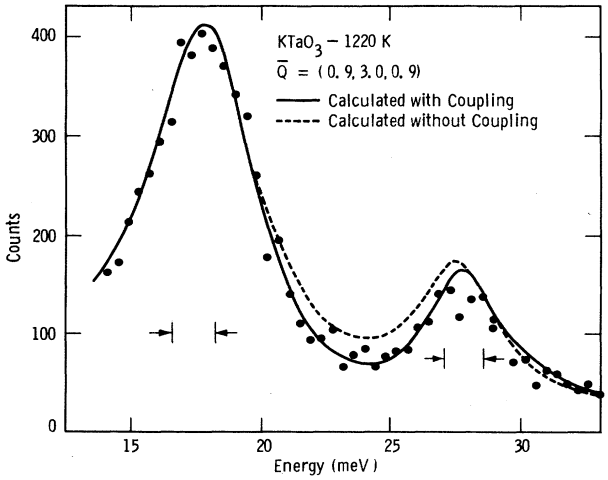

FIG. 3. Typical scattering profile measured at 1220 K of the two lowest frequency transverse-optic modes (TO_1 and TO_2) with Σ_4 symmetry. The solid line and dashed line represent the profiles calculated using parameters obtained from a least-squares fit of the data with and without anharmonic coupling between the modes. The instrumental resolution width is indicated by the arrows.

that even at 1220 K the TA and TO_1 modes remain underdamped and the scattering profiles give no direct evidence for anharmonic mode coupling. On the other hand both the TO_1 and TO_2 branches of Δ_5 and Σ_4 symmetry show some evidence of anharmonic coupling. Figure 3 shows typical scattering profiles for the TO_1 and TO_2 modes. In $KTaO_3$, at high temperatures there is only limited overlap of the mode response functions and the observed line shapes show little asymmetry. However, at 1220 K the TO_1 mode becomes sufficiently broadened to overlap with the TO_2 mode. The net result is that an optimum fit of the scattering profile is achieved only when mode interference is included in the calculation of the scattering profile.[26,29] The solid line in Fig. 3 is the result of such an analysis. The dashed line, shown in the figure for comparison is the result of a best fit calculation without mode interference. In contrast to the transverse branches, the longitudinal branches exhibit only normal (negative) energy shifts.

A systematic study of the temperature dependence of phonon frequencies at the Γ, X, M, and R points of the Brillouin zone was performed and the results are shown in Fig. 4. Many modes show a positive energy shift with increasing temperature. This behavior, which contrasts with the usual effect of lattice anharmonicity, can be accounted for on the basis of the present model. For this purpose the harmonic and nonlinear parameters K_{OB} and $K_{OB,B}$ were determined self-consistently[19] using Eqs. (1)–(3), in such a way as to reproduce the observed temperature dependence of the ferroelectric mode ($TO_1-\Gamma$) frequency. This procedure converges to $K_{OB}=341.8e^2/a^3$ and $K_{OB,B}=36.48\times10^4e^2/a^5$. The corresponding temperature dependence of $K_{OB}(T)$ is shown in Fig. 5. With the values of $K_{OB}(T)$ taken from this curve, the zone-center and zone-boundary phonon frequencies are calculated as a function of temperature. The results are shown as solid lines in Fig. 4. The agreement with the experimental values obtained for the ferroelectric mode in the whole temperature range is a nontrivial consequence of the self-consistent calculation. The three next-largest shifts [i.e., those of the modes TA(X), TA(M_3'), and $TO_2(X)$] are also fairly well described by the theory. All other calculated phonons do not shift significantly with temperature. In particular the model does not describe the relatively small upward shifts with increasing temperature of the modes TA(R), $TO_1(X)$, $TO_2(\Gamma)$, and Γ_{25}, or the downward shifts of the longitudinal frequencies at X and M. Note that these last modes are the only ones which show a significant negative shift. Thus the model, based on the temperature dependence of *only* the ferroelectric TO_1 mode, describes surprisingly well most modes with positive temperature shifts. The results of calculations of the dispersion curves which undergo the largest changes with temperature are shown for 20, 300, and 1200 K in Fig. 2 and compared with the experimental data.

The model is able to describe only the temperature dependence of modes which involve oxygen displacements along the direction of their neighboring Ta ions, since only these modes can be affected by the nonlinear

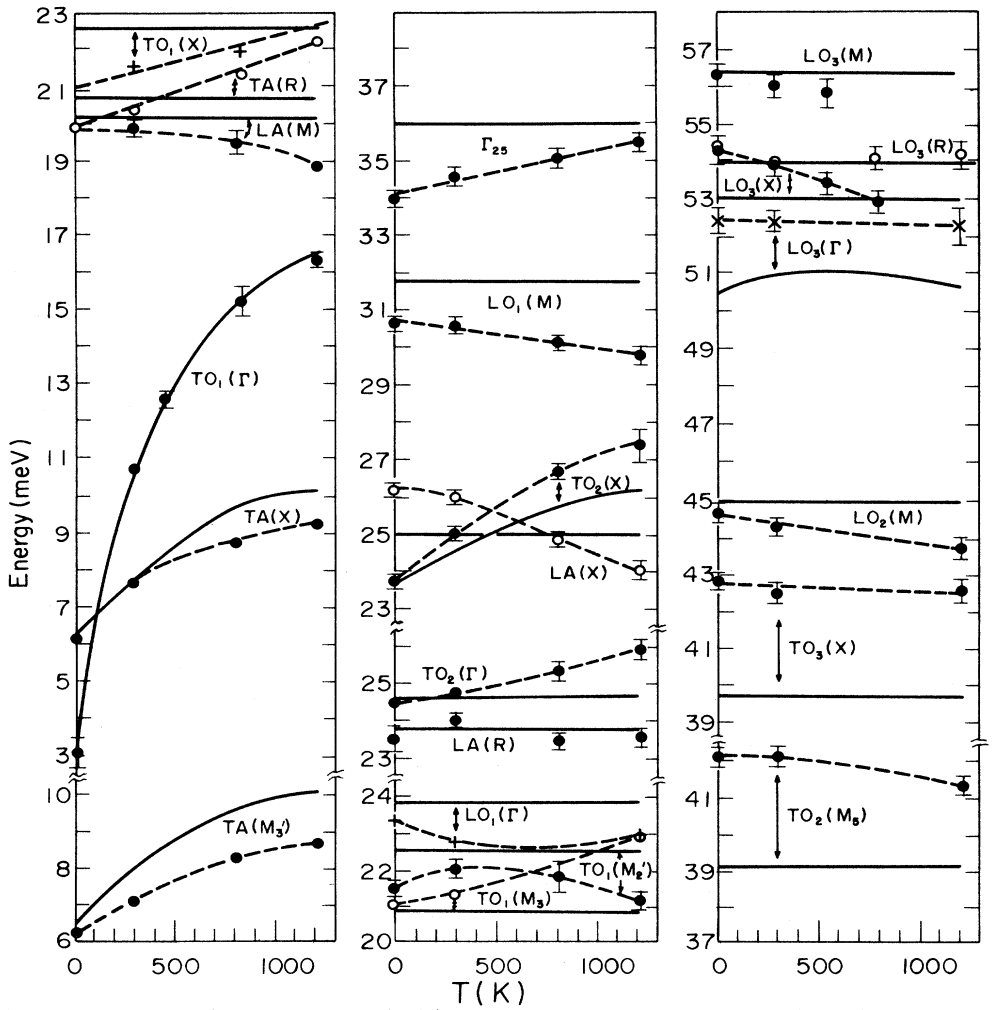

FIG. 4. Temperature dependence of zone-center and high-symmetry zone-boundary modes. The dashed lines are guides to the eye for the experimental data. The solid lines are calculated from the model described in the text.

coupling $K_{OB,B}$. This coupling gives rise to the temperature dependence of the effective harmonic parameter $K_{OB}(T)$ as shown in Eq. (1). The comparison between the experimental data and the model calculations as shown in Figs. 2 and 4 confirms that this mechanism is responsible for the most important changes in the dispersion curves. This particular model, however, ignores all other anharmonic mechanisms, such as third-order anharmonicity, which gives rise to negative energy shifts and to phonon damping. The small degree of damping observed in $KTaO_3$ appears to justify the neglect of these other mechanisms.

V. RAMAN SCATTERING

Raman scattering originates in the frequency modulation of the crystal electronic polarizability due to anharmonic electron-ion interactions. In crystals with all ions at inversion centers, such as $KTaO_3$, only two-phonon processes are Raman active. The second-order Raman tensor is obtained as the thermal average, with respect to

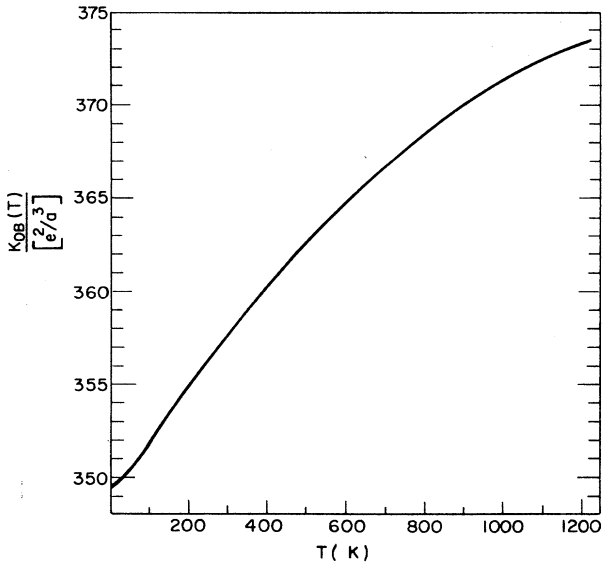

FIG. 5. Self-consistent temperature dependence of $K_{OB}(T)$, the B component of the quasiharmonic core-shell interaction at the oxygen ion.

the two-phonon density-of-states, of products of two polarizability coefficients $P_{\alpha\beta}(q,j;q,j')$. These are the second-order coefficients in the expansion of the polarizability tensor in terms of normal mode coordinates. Within the shell-model formalism, the $P_{\alpha\beta}(q,j;q,j')$ can be obtained in terms of nonlinear intraionic interactions.[35] The Raman tensor is then expressed as a quadratic combination of functions of the shell normal displacements where the combination coefficients are related to the nonlinear coupling constants. The calculation of the Raman tensor is a very sensitive test of both the phonon eigenvectors and frequencies over the whole Brillouin zone and of the polarizability mechanism chosen.

We consider the Raman scattering corresponding to the complete intraionic electron-phonon interaction at the oxygen site as described previously. In spite of its four independent nonlinear terms, the strongest component of the Raman tensor, i.e., the A_{1g} component, arises as a combination of only two independent contributions.[19] The coefficient of one of them, namely, $I^B_{A_{1g}}$, is a quadratic form of $K_{OB,B}$ and $K_{OB,A}$, while the coefficient of the other, $I^A_{A_{1g}}$, is quadratic in $K_{OA,A}$, $K_{OB,A}$, and $K_{OA,A'}$.

Both contributions are shown in the upper part of Fig. 6 in such a way that their absolute maxima coincide and with an arbitrary scale with respect to the experimental A_{1g} component (solid line). $I^B_{A_{1g}}$ (dashed line) reproduces almost all the features of the experimental spectrum.[8,9] Due to the refinement of the phonon fit this result is also significantly improved as compared to previous calculations.[19] On the other hand, $I^A_{A_{1g}}$ (dotted line) is completely different from the experimental spectrum and its combination with $I^B_{A_{1g}}$ (including a mixing term not shown here) does not lead to any significant improvement of the results. Notice also, on the right-hand side of the A_{1g} spectrum in Fig. 6, a scale which corresponds to $I^A_{A_{1g}}$ re-

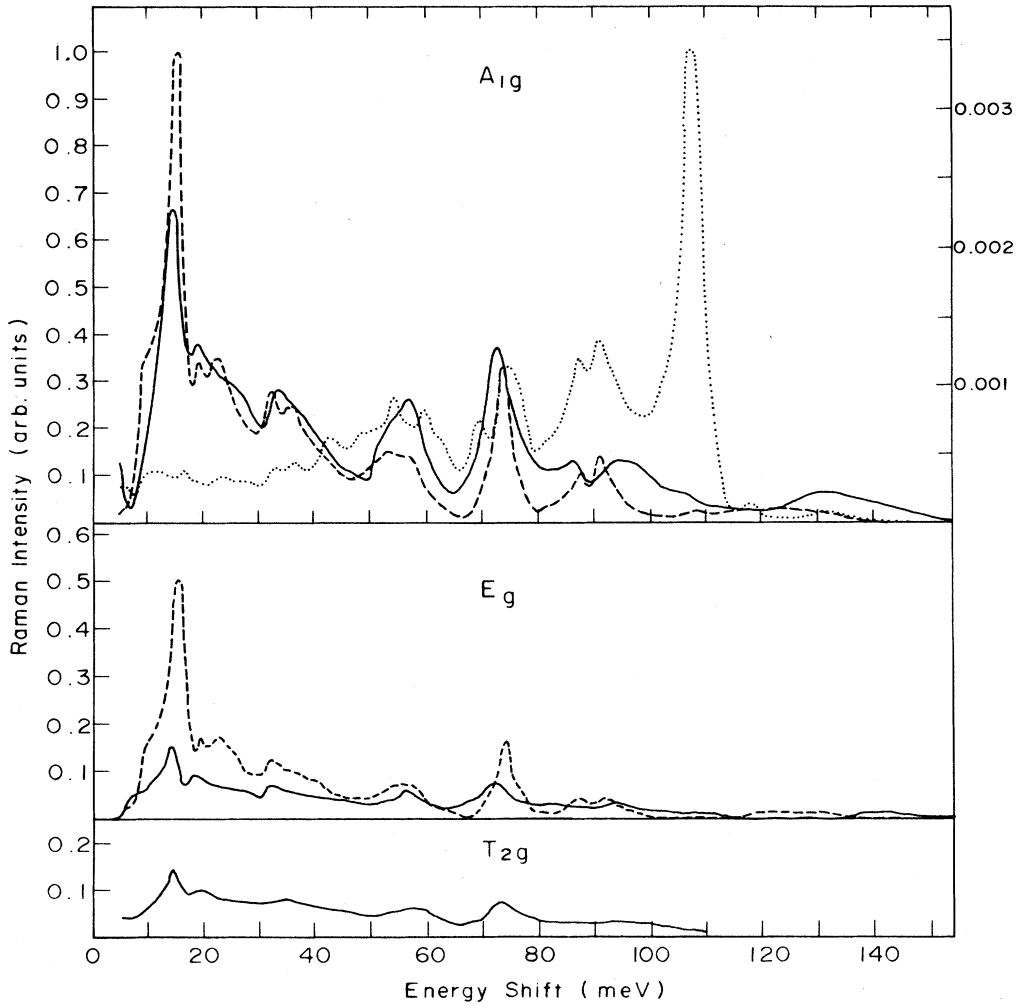

FIG. 6. Irreducible components of the Raman spectra of $KTaO_3$, plotted with the same intensity scale. Solid line: experiment (Refs. 8, 9, and 19). Dashed line: calculated with $K_{OB,B}$ as the only nonlinear parameter (which does not contribute to the T_{2g} component). Dotted line: the only other independent contribution to the A_{1g} component, plotted with the magnified scale shown on the right.

ferred to the maximum of $I^B_{A_{1g}}$ for equal values of the four anharmonic parameters. Since $I^A_{A_{1g}}$ is about 3 orders of magnitude weaker than $I^B_{A_{1g}}$ in this isotropic case, the resulting combined spectrum does not show any significant difference from $I^B_{A_{1g}}$.

In the case of the E_g component, each of the four nonlinear terms independently contributes to the Raman tensor. However, again only the contribution of $K_{OB,B}$ reproduces the experimental spectra. This is shown by the dashed line in the middle part of Fig. 6, drawn with the same intensity scale used for the contribution of $K_{OB,B}$ to A_{1g}. A very satisfactory agreement is observed. Also the intensity ratio with the A_{1g} component is in agreement with the experimental ratio except for the strongest peak. The other three intraionic contributions to E_g are so weak that the spectrum obtained for the isotropic case is practically the same as the contribution shown in Fig. 6. An improvement of the E_g to A_{1g} ratio with the help of the parameter $K_{OB,A}$ can be achieved only for values of $K_{OB,A}$ higher than $K_{OB,B}$ which in turn spoils the fit of the A_{1g} component due to the influence of $I^A_{A_{1g}}$.

The T_{2g} component of the Raman tensor contains only contributions of the interactions corresponding to $K_{OB,A}$ and $K_{OA,A'}$. Both calculated contributions are quite different from the experimental spectrum. They also are negligibly small compared with A_{1g} or E_g when the isotropic case is considered.

VI. SPECIFIC HEAT

Figure 7 shows the low-temperature specific heat C_v of $KTaO_3$ as measured some years ago by Lawless[36] (curve A) and more recently by Salce *et al.*[37] (curve B). The C_v/T^3 versus T^2 semilogarithmic plot is chosen as a very sensitive way to display the C_v/T^3 maximum. This maximum may be attributed to low-lying vibrational modes which remain populated at low temperatures. In order to take into account the softening of the low-frequency modes with decreasing temperature, a calculation of C_v was performed by using a frequency distribution $g(\omega)$ recalculated for each temperature. The result is indicated by curve C in Fig. 7. The specific heat calculated with the room temperature $g(\omega)$ is shown for comparison as curve D. It is seen that the modes that soften shift the C_v/T^3 maximum to lower temperatures.

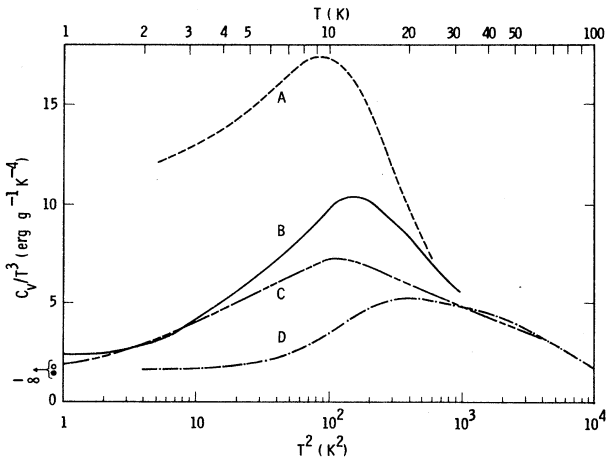

FIG. 7. Lattice specific heat: curve A (— — —) (Ref. 36) and curve B (——) (Ref. 37) are experimental data. The calculated temperature-dependent frequency distributions is indicated by curve C (———); the room temperature $g(\omega)$ is shown for comparison, curve D (—·—·—·). Value of C_v/T^3 for $T\rightarrow 0$ K calculated from the elastic constants at 0 K: experimental (Refs. 13 and 33) (○) and obtained from model parameters (●).

In order to avoid errors arising from the numerical integration of the low-frequency part of $g(\omega)$ near $T=0$ K, an interpolation formula

$$g(\omega)=\frac{3}{\omega_0^3}\omega^2+b\omega^4+c\omega^6 \tag{4}$$

was used well below the ferroelectric soft-mode frequency, where the low-q acoustic modes are the dominant contributions to $g(\omega)$. ω_0 is the Debye frequency determined by de Launay's procedure;[38] b and c are determined by fitting expression (4) to the $g(\omega)$ histogram in the interpolation range.

Also plotted in Fig. 7 is the limiting value of C_v/T^3 as $T\rightarrow 0$ K, calculated from the values of the elastic constants, using the method of de Launay. Experimental values for the elastic constants C_{11} and C_{44} were obtained from ultrasonic measurements at low temperature. A value $C_{12}=1.35\times 10^2$ dyn/cm^2 was deduced from the low-temperature slope of the TA(Σ_3) mode.[13] The corresponding specific-heat value is shown as (○) on the left-hand side of Fig. 7. The point marked (●) slightly below (○) is calculated using de Launay's technique and elastic constant values obtained from the shell-model parameters. These latter values are temperature independent since they do not depend on electronic polarizabilities.

Both calculated curves, C and D in Fig. 7, extrapolate to the point marked (●). The result of the calculation with the temperature-dependent frequency distribution (curve C) is in fairly good agreement with the measurements of Salce *et al.*[37] The higher values of C_v measured by Lawless[36] suggest the presence of other types of contributions to the specific heat for his sample. One plausible mechanism would involve the interaction of the ferroelectric soft mode with defects. Since the soft mode is almost unstable at 0 K, isolated point defects may freeze a polar configuration over a certain correlation volume. Such an effect has been observed with lithium substituted for potassium.[39] The thermal activation energy required to switch such polar clusters would lead to an increase of the observed heat capacity with respect to the perfect lattice case, consistent with the low-temperature discrepancy shown in Fig. 7.

VII. CONCLUSION

We have presented here the results of a detailed study of the temperature dependence of phonon modes in cubic

$KTaO_3$ and have shown how a shell model, extended to include a fourth-order core-shell interaction at the oxygen ion, is capable of describing many of the phonon shifts and, in particular, the second-order Raman spectrum.

From the results of the Raman-scattering calculations it is not possible to assert whether or not the intraionic nonlinear oxygen polarizability is actually anisotropic. This is due to the fact that the spectra obtained are fairly insensitive to the parameters $K_{OB,A}$, $K_{OA,A}$, and $K_{OA,A'}$ as long as these are not much greater than $K_{OB,B}$. In order to verify whether a model with an isotropic polarizability would be able to reproduce also the phonon thermal shifts, we have analyzed the effect on the dispersion curves of the simultaneous variation of K_{OA} and K_{OB}, with the ratio K_{OB}/K_{OA} held at the value determined at room temperature. Values for these parameters were chosen which exactly fit the experimental values of $\omega_{TO1}(\Gamma)$ at the various temperatures measured. The resulting phonon frequencies did not show any significant deviation from the calculated values in Fig. 4, which correspond to taking $K_{OB}(T)$ as the only temperature-dependent parameter. Although performed for an anisotropic harmonic coupling, this test is indicative of what can be expected from an isotropic variation of the oxygen core-shell coupling. However, within a self-consistent treatment of the complete intraionic interaction at the oxygen ion, the quasiharmonic parameter $K_{OB}(T)$ and $K_{OA}(T)$ will exhibit different temperature dependences. Even for isotropic intraionic interaction, we have $\langle W_{OB}^2 \rangle \neq \langle W_{OA}^2 \rangle$ due to the tetragonal symmetry of the oxygen site. Moreover, a previous calculation with an isotropic harmonic model has led to a self-consistent behavior of $\langle W_{OB}^2 \rangle$ versus T, which does not reproduce the form of $\omega_{TO_1}^2(T)$ versus T (dotted line in Fig. 2 in Ref. 19).

Even if there is no conclusive evidence that the intraionic electron-ion interaction at the oxygen is anisotropic, it is clear from our separate analysis of each core-shell coupling distinguishable by symmetry that only the nonlinear polarization of the oxygen along the Ta—O—Ta chains can account for the Raman scattering and the most important phonon shifts, particularly the ferroelectric soft mode. In fact the TA and TO modes propagating in the $\langle 100 \rangle$ directions can be described[40,41] by the transverse modes of a pseudo-one-dimensional diatomic chain with a rigid cation and nonlinearly polarizable anion, corresponding to $[TaO_3]^-$. The electronic polarizability of the anion includes effectively the O^{2-} polarizability along a Ta—O—Ta chain. This simplified version can be handled analytically in the self-consistent phonon approximation and is able to describe correctly the temperature behavior of the [100] modes shown in Fig. 2.

Also a calculation of the electronic structure of O^{2-} in a Watson sphere[42] indicates that an anisotropic environment of the O^{2-} ion would lead to an enhancement of the volume dependence of its polarizability. An additional anisotropic enhancement along the Ta—O—Ta chains arises[42] if the p states of O^{2-} hybridize with the d states of the neighboring Ta.

ACKNOWLEDGMENTS

The authors wish to acknowledge the late Dr. Heinz Bilz for his many contributions and constant encouragement. R.L.M. is particularly indebted to Dr. Bilz for his hospitality and helpful discussions at Max-Planck-Institut für Festkörperforschung (MPIF), Stuttgart, during the writing part of this paper. Dr. W. Kress is also acknowledged for his contributions during this period. We are grateful to Dr. A. Linz, MIT, for providing the excellent $KTaO_3$ sample and to Dr. J. Bouillot (ILL) and Professor R. P. Lowndes (Northeastern University) for assistance during the early measurements. The work at the Brookhaven National Laboratory was supported by the Division of Materials Sciences, Office of Basic Energy Sciences, U.S. Department of Energy under Contract No. DE-ACBS-76CH00016. C.H.P. gratefully acknowledges partial support from the Alexander von Humboldt Foundation while at MPI, Grenoble. C.H.P., R.C., and H.B. appreciate partial travel support under North Atlantic Treaty Organization (NATO) Grant No. 1360. The work at Northeastern University received support from National Science Foundation (NSF) Grant No. DMR-75-06789 and No. DMR-86-04706.

*Present address: Westinghouse Research and Development Center, Pittsburgh, PA 15235.

†Present address: Department of Physics, University of Keele, Keele, Staffordshire ST5 5BG, United Kingdom.

‡Present address: Instituto de Física Rosario, 27 de Febrero 210Bis, 2000 Rosario, Argentina.

[1]F. Jona and G. Shirane, *Ferroelectric Crystals* (Macmillan, New York, 1962), pp. 108–254.

[2]G. Shirane, H. Danner, A. Pavlovic, and R. Pepinsky, Phys. Rev. **93**, 672 (1954).

[3]G. Rupprecht and R. O. Bell, Phys. Rev. **135**, A748 (1964).

[4]R. C. Miller and W. G. Spitzer, Phys. Rev. **129**, 94 (1963).

[5]A. S. Barker, Phys. Rev **145**, 391 (1966).

[6]C. H. Perry and T. F. McNelly, Phys. Rev. **154**, 456 (1967).

[7]K. F. Pai, T. J. Parker, N. E. Tornberg, R. P. Lowndes, and W. G. Chambers, Infrared Phys. **18**, 327 (1978); K. F. Pai, T. J. Parker, and R. P. Lowndes, Ferroelectrics **21**, 337 (1978).

[8]W. G. Nilsen and J. G. Skinner, J. Chem. Phys. **47**, 1413 (1967).

[9]C. H. Perry, J. H. Fertel, and T. F. McNelly, J. Chem. Phys. **47**, 1619 (1967).

[10]P. Fleury and J. Worlock, Phys. Rev. **174**, 613 (1968).

[11]Y. Yacoby and A. Linz, Phys. Rev. B **9**, 2723 (1974).

[12]G. Shirane, R. Nathans, and V. J. Minkiewicz, Phys. Rev. **157**, 396 (1967).

[13]J. D. Axe, J. Harada, and G. Shirane, Phys. Rev. B **1**, 1227 (1970).

[14]R. Comès and G. Shirane, Phys. Rev. B **5**, 1886 (1972).

[15]H. Vogt and H. Uwe, Phys. Rev. B **29**, 1030 (1984).
[16]K. A. Müller and H. Burkard, Phys. Rev. B **19**, 3593 (1979).
[17]J. F. Scott, Rev. Mod. Phys. **46**, 83 (1974).
[18]A. S. Barker, Jr. and J. J. Hopfield, Phys. Rev. **135**, A1721 (1964).
[19]R. Migoni, Ph.D. thesis, University of Stuttgart, 1977; R. Migoni, H. Bilz, and D. Bäuerle, Phys. Rev. Lett. **37**, 1155 (1976).
[20]R. Migoni, H. Bilz, and D. Bäuerle, in *Lattice Dynamics,* edited by M. Balkanski (Flammarion, Paris, 1977), p. 650.
[21]Y. Fuju and T. Sakudo, J. Phys. Soc. Jpn. **41**, 888 (1976).
[22]J. P. Ansermet, D. Rytz, A. Châtelain, U. T. Höchli, and H. E. Weibel, J. Phys. C **14**, 4541 (1981).
[23]R. A. Cowley, Phys. Rev. **134**, A981 (1964).
[24]W. G. Stirling, J. Phys. C **5**, 2711 (1972).
[25]W. G. Stirling and R. Currat, J. Phys. C **9**, L519 (1976).
[26]C. H. Perry, H. Buhay, A. M. Quittet, and R. Currat, in *Proceedings of the International Conference on Lattice Dynamics, Paris, 1977,* edited by M. Balkanski (Flammarion, Paris, 1978), p. 677.
[27]H. Buhay, C. H. Perry, R. Currat, and A. M. Quittet, Bull. Am. Phys. Soc. **50**, 527 (1985).
[28]B. Dorner, B. Hennion, and J. Prevot (private communication).
[29]J. Harada, J. D. Axe, and G. Shirane, Phys. Rev. B **4**, 155 (1971).
[30]L. Gnininvi and J. Bouillot, Ferroelectrics **15**, 173 (1977).
[31]M. J. Cooper and R. Nathans, Acta Crystallogr. **23**, 357 (1967).
[32]J. Harada, J. D. Axe, and G. Shirane, Acta Crystallogr. Sect. A **26**, 608 (1970).
[33]H. H. Barret, Phys. Lett. **26A**, 217 (1968).
[34]R. A. Cowley, Proc. R. Soc. London, Ser. A **268**, 121 (1962).
[35]A. D. Bruce and R. A. Cowley, J. Phys. C **5**, 595 (1972).
[36]W. N. Lawless, Phys. Rev. B **14**, 134 (1976); *ibid.* **17**, 1458 (1978).
[37]B. Salce, R. Calemczuk, E. Bonjour, R. L. Migoni, and L. A. Boatner, in *Proceedings of the Second International Conference on Phonon Physics, Budapest, 1985,* edited by J. Kollár, N. Kroó, N. Menyhárd, and T. Siklós (World Scientific, Singapore, 1986), p. 979.
[38]J. de Launay, in *Solid State Physics,* edited by F. Seitz and D. Turnbull (Academic, New York, 1956), Vol. 2, pp. 219–313.
[39]W. N. Lawless, D. Rytz, and U. T. Höchli, J. Phys. C **17**, 2609 (1984).
[40]H. Bilz, A. Bussmann, G. Benedek, H. Büttner, and D. Strauch, Ferroelectrics **25**, 339 (1980).
[41]A. Bussmann-Holder, H. Bilz, D. Bäuerle, and D. Wagner, Z. Phys. B **41**, 353 (1981).
[42]A. Bussmann, H. Bilz, R. Ronspiess, and K. Schwarz, Ferroelectrics **25**, 343 (1980).